Letter Vol. 46, No. 5 / 1 March 2021 / Optics Letters 929

Optics Letters

Spectral broadening of 112 mJ, 1.3 ps pulses at 5 kHz in a LG_{10} multipass cell with compressibility to 37 fs

Martin Kaumanns,[1,*] Dmitrii Kormin,[1] Thomas Nubbemeyer,[1] Vladimir Pervak,[1] and Stefan Karsch[1,2]

[1]Ludwig-Maximilians-Universität München, Am Coulombwall 1, 85748 Garching, Germany
[2]Max-Planck-Institut für Quantenoptik, Hans-Kopfermann-Str. 1, 85748 Garching, Germany
*Corresponding author: martin.kaumanns@physik.uni-muenchen.de

Received 4 December 2020; revised 22 January 2021; accepted 24 January 2021; posted 25 January 2021 (Doc. ID 416734); published 16 February 2021

The first-order helical Laguerre–Gaussian mode (also called donut mode) is used to improve the energy throughput of nonlinear spectral broadening in gas-filled multipass cells. The method proposed in this Letter enables, for the first time to the best of our knowledge, the nonlinear spectral broadening of pulses with energies beyond 100 mJ and is suitable for an average power of more than 500 W while conserving an excellent spatio-spectral homogeneity of ∼98% and a Gaussian-like focus profile. Additionally compressibility from 1.3 ps to 37 fs is demonstrated. © 2021 Optical Society of America

https://doi.org/10.1364/OL.416734

Gas-filled multipass cells have recently become a well-established tool for nonlinear spectral broadening and pulse compression into the femtosecond regime. Based on multipass cells, laser systems with sub-100 fs pulses and average powers up to 1 kW have been demonstrated [1]. Also pulses with energies in the tens of millijoules regime can be spectrally broadened in multipass cells while providing excellent beam quality and compressibility to the tens of femtoseconds regime [2–4]. Additionally high transmission values beyond 90% [2] and single stage compression factors up to 40 have been realized [5].

These exciting properties made nonlinear compression based on multipass cells a promising candidate for future high repetition rate, high energy femtosecond sources. Such sources are of high interest for kilohertz laser wakefield acceleration experiments [6] or high photon-flux Thomson x ray sources [7]. Yet a significant increase of supported pulse energy toward the sub-joule regime is necessary for gas-filled multipass cells in order to allow a straightforward application within these fields.

The throughput energy of gas-filled multipass cells is limited by the damage threshold of the cell mirrors and the ionization threshold of the gas [2]. The ionization leads to drastic absorption of laser power or distorts the propagating mode to a degree that subsequently causes damages of cell optics. Longer cells can be used to obtain larger eigenmodes and, therefore, higher throughput energies [2], yet even for cells with a length of ∼8 m, demonstrated pulse energies do not exceed 40 mJ in argon [3].

In this Letter, we experimentally exploit a first-order donut mode for the energy scaling of a multipass cell. We present the nonlinear spectral broadening of pulses with energies of more than 100 mJ and a throughput over 95% at a repetition rate of 5 kHz and show the compressibility from 1.3 ps to 37 fs. This corresponds to the highest energy spectrally broadened in a mode preserving system known to the authors.

Gas-filled multipass cells preserve their input spatial mode by a dephasing mechanism [8]. In the following, this mechanism is briefly introduced for helical *Laguerre–Gaussian* modes LG_{lm}:

$$LG_{lm} = LG_{00}\left(\frac{r}{w}\right)^{|l|}\mathbb{L}_m^{|l|}\left[\frac{2r^2}{w^2}\right]e^{-\mathrm{i}(|l|+2m)\zeta+\mathrm{i}l\phi}, \quad (1)$$

with the Gaussian mode LG_{00} defined using the cylindrical coordinates (radius r, angle ϕ), the generalized Laguerre polynomial $\mathbb{L}$, the mode radius w, and the Gouy phase shift of the Gaussian mode ζ. The modes LG_{l0} are also called *l-order donut mode* due to their donut-like transverse intensity distribution.

If a fundamental Gaussian input is subject to a weak spatially distributed distortion like, e.g., Kerr lensing in a nonlinear medium, some energy will be coupled into higher order modes LG_{lm}. The higher order modes co-propagate with the Gaussian mode while shifting in phase by the value $(|l|+2m)\zeta$ relative to the Gaussian [see Eq. (1)]. This dephasing prevents a constructive buildup of higher order components during the propagation in, e.g., a nonlinear medium, thus ensuring that only the Gaussian mode is preserved.

The mode preserving mechanism for high-order inputs can be deduced from this picture: assuming a first-order donut mode LG_{10} as input, the relative phase shift of the input has a value of ζ. All non-phase-matched modes LG_{lm} that accumulate a different phase shift $(|l|+2m)\zeta \neq \zeta$, i.e., all modes except the inverted donut mode LG_{-10} are, therefore, dephasing during propagation, and their buildup is prevented. However, any resulting mode consisting of LG_{10} and LG_{-10} components would violate the rotational intensity symmetry expected from Kerr induced distortions of a rotationally symmetric input beam [9]. Thus, the coupling into the LG_{-10} mode is negligible, and

multipass cells are expected to show close to ideal mode preserving properties for input modes that approximate the first-order donut mode LG_{10} [3,10] ([11], p. 123). In addition, the peak intensity of the first-order donut mode LG_{10} is about 2.7 times lower than the peak intensity of the equivalently propagating Gaussian mode LG_{00} [11, p. 124] while the critical power increases by a factor of 4 [12]. In a related concept, a reduction of peak intensity in an optical fiber was obtained by using a higher order mode [13].

For the experimental realization, the Yb:YAG thin-disk amplifier described in [14], in combination with a modified front end based on a fiber laser oscillator (*Menlo YLMO*), is used as a source. The system delivers up to 200 mJ of pulse energy at 5 kHz with 1.3 ps full width at half-maximum (FWHM) pulse duration. Its spectrum is centered at 1030 nm with a bandwidth of 1.3 nm, and its $1/e^2$ diameter (for brevity simply referred to as *diameter* in the following) is 16 mm. A low-order wave plate, in combination with two thin film polarizers, is used to control the input power into the multipass cell and provide a linearly polarized input.

The Gaussian mode of the source laser is converted to a first-order donut mode by placing an optical vortex plate *VP1* with a topological charge of $l = 1$ into the beam (*VL-246-J-Y-E* produced by *HOLO/OR Ltd.*; manufacturer specification: transmission close to 100%, conversion efficiency ∼95%). Optical vortex plates or spiral phase plates are AR-coated fused silica plates with a thickness of 2–3 mm and a spiral staircase-like structure etched onto the surface. The surface structure creates a helical phase delay that is a key property of the LG_{10} donut mode. While the intensity pattern still follows a Gaussian shape in the near field, the LG_{10}-like phase causes a donut-like intensity pattern in the far field, and the beam can be approximately treated as linearly polarized LG_{10} mode in the following. As depicted in Fig. 1(a), the beam is then coupled into a concentric Herriott-type multipass cell filled with 250 mbar of argon similar to the one published in [2]. The cell consists of two concave rectangular mirrors with a radius of curvature (RoC) of 4 m, a size of 300 × 130 mm^2 and a reflectivity of >99.9% as well as a group delay dispersion (GDD) of $|GDD| < 50$ fs^2 between 965 and 1100 nm placed in a 9 m long and 0.68 m wide low pressure chamber with 6 mm thick plane fused silica windows for in- and outcoupling. The input beam is mode matched to the eigenmode of the cell by a telescope system consisting of a 3 m RoC concave, 2 m RoC convex, and 10 m RoC concave mirror summarized as effective mirror 1 in the schematic in Fig. 1(a). The angle of incidences on the mirrors used for the input telescope are carefully optimized to remove any leftover astigmatism of the input beam. Also the usage of plane instead of wedged input windows prevents additional angular wavelength chirp. A plane mirror (diameter 25 mm) placed in front of the large rectangular mirror 3 steers the beam into the cell.

After 40 foci, the beam is coupled out by a second mirror with a diameter of 25 mm. An approximate collimation is performed by using a concave RoC of 20 m for outcoupling schematically depicted as the collimation mirror 4 in Fig. 1(a). After the beam is coupled out of the cell, a second vortex plate *VP2* identical to the plate used for the input is placed into the beam. By flipping the orientation of the etched surface in comparison to the input plate, the initially introduced helical phase is compensated, and the output beam acquires a flat wavefront. The propagation after flattening the wavefront does not resemble the propagation

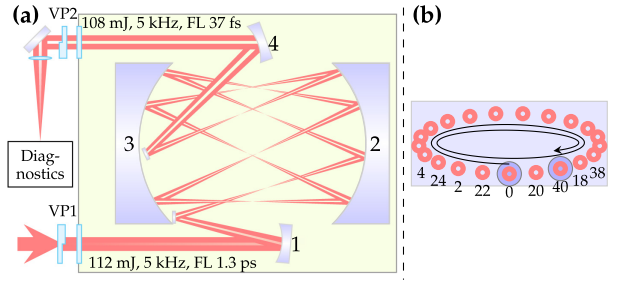

Fig. 1. (a) Scheme of the multipass cell setup (side view) with energies, repetition rates, and Fourier limits (FL) of the input and output pulse. VP1 and VP2 denote the input and output vortex plates. Mirrors 1 and 4 are substitutes for the input mode matching and output collimation optical systems. Mirrors 2 and 3 are concave 4 m RoC. The separation between mirrors 2 and 3 is about ∼1.96 times their RoC (≈ 7.8 m). (b) Beam pattern on mirror 3. The spots are labeled according to the accumulated passes through the focus. After 40 passes, the beam is picked by an outcoupling mirror.

of a perfect Gaussian beam but rather exhibits a donut-shaped intensity pattern in the near field and a Gaussian-like far field that can be used for experiments. Between these two planes, the beam develops a large pedestal with a pronounced intensity spike in the center, and care must be taken to avoid any clipping or damages.

The distance of nearly 8 m between the Herriott cell mirrors 2 and 3 is chosen such that the Gaussian eigenmode LG_{00} for a wavelength of 1030 nm has a beam diameter of about 5.9 mm on the cell mirrors and about 890 µm in the focus. The measured damage threshold of the cell mirrors is on the order of 1 J/cm^2, and argon is expected to ionize at about 40 J/cm^2 for the given input pulse [2]. The maximum theoretically possible throughput energy for the Gaussian eigenmode is, therefore, 125 mJ. The corresponding first-order donut eigenmode LG_{10} of the presented cell features a $1/e^2$ beam diameter of 8.9 mm on the cell mirrors and 1.3 mm in the focus. Due to the 2.7 times lower peak intensity, the maximum theoretically possible throughput energy for the LG_{10} eigenmode increases to more than 330 mJ.

112.4 mJ of pulse energy (average power of 561.8 W) is sent into the cell and spectrally broadened. The measured output pulse energy at this working point is 107.8 mJ (average power of 539 W). This corresponds to a transmission of 95.9%, which is a common value for multipass systems [1,2,4]. Assuming ideal mode matching, we expect a peak fluence of 0.3 J/cm^2 on the mirrors. The input energy represents only a third of the maximum theoretically possible throughput energy, allowing for high robustness against mode matching errors, mirror imperfections, or the development of hot spots in the beam. After outcoupling, the beam is attenuated by two fused silica wedges and focused for the following analysis (if not mentioned otherwise). The focusing system for the slightly divergent output consists of a convex lens with a focal length of 1 m placed close to the vortex plate *VP2* and a 0.15 m concave lens after an additional propagation of 963 mm. The focal plane of this system is at the distance of about 1.77 m from the concave lens.

Figures 2(a) and 2(b) show the focal spot profiles of the output beam without and with the compensating vortex plate *VP2*. Figure 2(a) represents a donut like shape as expected for a LG_{10} output mode. Figure 2(b) has a Gaussian-like shape

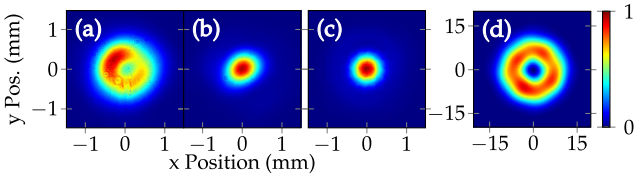

Fig. 2. Output profiles of the multipass cell. Depicted are the focal spots measured at the energy of 107.8 mJ (a) without and (b) with the compensating output vortex plate *VP2*. The diameters are 1.86 mm and 1.09 mm, respectively. (c) shows the numerically calculated best-case focal spot profile (diameter 0.96 mm) and (d) the profile at the plane of *VP2* (diameter 26.4 mm) obtained by backpropagating the profile (a) with an ideal LG_{10} spiral wavefront.

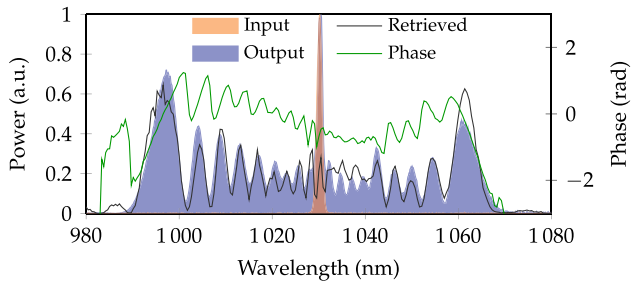

Fig. 3. Measured input (orange) and output (blue) spectra. Additionally depicted are the retrieved spectrum (black) and phase (green) from the SHG-FROG measurement of the compressed pulse.

with a weak pedestal surrounding the main beam. We expect the non-compensated output mode to feature a LG_{10}-like spiral wavefront that can be flattened almost perfectly with the first-order vortex plate *VP2*. The focus profile in Fig. 2(b) is, hence, assumed to be close to the diffraction limit. To support this claim, we numerically backpropagated the profile shown in Fig. 2(a) assuming the ideal LG_{10} wavefront using the Hussar framework [15] (grid size 60 × 60 mm^2, 4096 × 4096 bins) to the plane of *VP2*. The resulting profile is shown in Fig. 2(d). We then flattened the wavefront by numerically adding the phase profile of the vortex plate and propagated the beam to the focus plane again obtaining the best-case focus shown in Fig. 2(c). The strong similarity between Figs. 2(b) and 2(c) support our claim of an almost diffraction limited focus with a peak intensity ratio between the best-case focus and the measured focus (*Strehl ratio*) of 88%. More than 70% of the beam energy is within the $1/e^2$ diameter of the measured compensated focus (for the ideal Gaussian mode 86.4%). This is similar to the expected value of 76.4% obtained by a numerical simulation of this concept ([11], p. 125).

The measured output spectrum with a Fourier limit of ∼37 fs and the measured input spectrum are depicted in Fig. 3 together with the spectral power and phase obtained from the pulse retrieval. The shape approximately follows the expected profile of self-phase modulation (SPM) known from multipass cells with a Gaussian mode (as, e.g., in [2]). The central peak is a consequence of low-intensity background in the input pulse, e.g., caused by amplified spontaneous emission or weak pre-/post-pulses. The broadening factor defined by the input Fourier limit divided by the output Fourier limit is approximately 35.

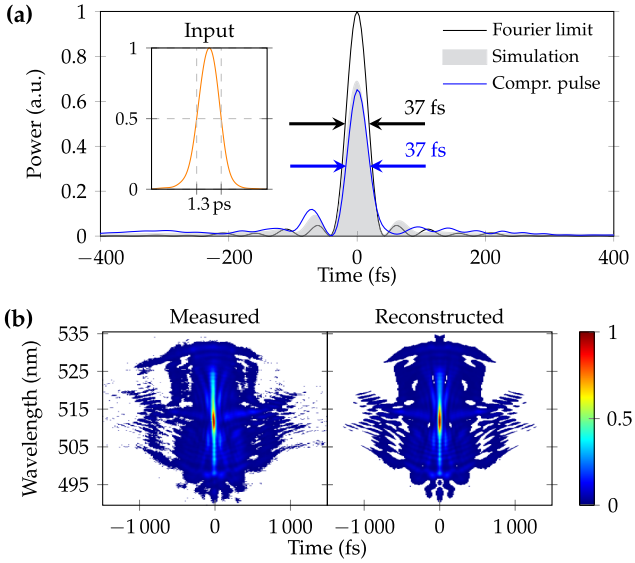

Fig. 4. (a) Fourier limited pulse calculated from the output spectrum shown in Fig. 3 (black) together with the retrieved compressed pulse (blue) and a simulation of the nonlinear compression (gray). The arrows mark the FWHM durations of the Fourier limited pulse (black) and the compressed pulse (blue). The measured input pulse and its FWHM duration is shown in the inset. (b) The measured (left) and the retrieved (right) SHG-FROG intensity for the compressed pulse in (a).

By inserting the known pulse shape $A(t)$ of the source system [see inset of Fig. 4(a)] into the SPM equation $I(\omega) \approx |\mathcal{F}[A(t)\exp(i\varphi|A(t)|^2)]|^2$, it was found that a nonlinear phase shift of $\varphi \approx 54$ rad yields the best overlap between the expected spectrum $I(\omega)$ and the measured spectrum shown in Fig. 3. The expected compressed pulse shape is deduced by removing the GDD phase component from the calculated spectrum $I(\omega)$ and plotted with the label *Simulation* in Fig. 4(a).

The theoretical nonlinear phase shift of the Gaussian eigenmode of this setup is 130 rad for 40 dispersion-free passes in 250 mbar of argon [16,17]. The presented setup based on a LG_{10} mode, therefore, reduced the effective nonlinear phase shift or equivalently the effective intensity of the setup by a factor of 2.4, which is in reasonable agreement to the previously introduced expected reduction of peak intensity by a factor of 2.7.

The experimental compression of the output beam was performed by guiding 0.1% of the output power (attenuation by two uncoated fused silica wedges) into a free-space chirped mirror compressor. The attenuation is necessary to avoid nonlinear contributions of air and possible damages of the used chirped mirrors. Also the beam was not focused but rather collimated with a 1:4 telescope after the multipass cell. The compression of the full output power requires a vacuum environment and bigger beam diameters. A suitable setup will be implemented in the future. To guarantee a well-behaved propagation through the chirped mirror compressor, the wavefront of the beam was not compensated, and the donut output mode was directly used. Only minor nonlinear distortions are expected even if the compensation is applied after the compression of the full output energy: a commercial 2 mm thick fused silica vortex plate with an aperture of 150 mm adds an insignificantly small

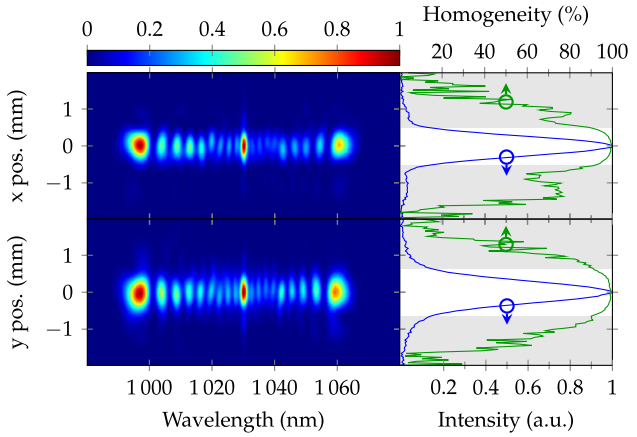

Fig. 5. Spatial wavelength distribution for the x and y axis of the output beam. The blue curve on the right shows the normalized sum along the wavelength axis of the image on the left. The white area marks the positions where this normalized sum is bigger than $1/e^2$. The green curve shows the corresponding homogeneity value.

maximum phase shift of 0.3 rad (donut mode diameter 75 mm, pulse energy 108 mJ, duration 37 fs).

After 12 bounces with a GDD of about $-500\ \mathrm{fs}^2$ per bounce and a total transmission of ∼99%, the compressed pulses are characterized by a single shot-type second-harmonic generation frequency resolved optical gating (SH-FROG) setup. The measured and retrieved FROG traces are shown in Fig. 4(b) while the retrieved spectrum and the retrieved phase are depicted in Fig. 3. The agreement between the retrieved and measured spectrum as well as a reasonably small SHG-FROG error of 1.3% on a 512×512 grid indicates a correct retrieval. The retrieved pulse is plotted in Fig. 4(a) together with the deduced Fourier limit of the output spectrum and the previously introduced simulated expected compression. All pulses shown in Fig. 4(a) are normalized for energy such that the pulse's peak values give a figure of merit for the compression quality. The obtained compression and the expected simulated compression feature peak values of 65.1% and 68.9%, respectively, of the Fourier limit peak power. Similarly good agreement is observed for the retrieved FWHM pulse duration (37 fs) and the simulated value (38 fs).

To measure the spatio-spectral homogeneity of the output beam, the vortex-compensated beam was focused into an imaging spectrometer (*Acton Research Corporation*), and the homogeneity value V was calculated following the definition used in [2]. The result is presented in Fig. 5. The intensity weighted homogeneities within the $1/e^2$ range of the depicted measurements are 98.3% for the x axis and 98.2% for the y axis and are above 90% within the complete $1/e^2$ diameter. These values are in close agreement with the results obtained for the fundamental Gaussian beam [2] and confirm that the usage of a first-order donut mode allows for high input energies while demonstrating excellent spatio-spectral homogeneity. As the SPM spectrum $I(\omega)$ is deduced from the temporal profile of the pulse $A(t)$, strong spatial pulse shape variations during the SPM-broadening would affect the spatio-spectral distribution of the output beam. Thus, a high spectral homogeneity can be also seen as indication of good spatiotemporal quality.

In conclusion, we demonstrated the nonlinear spectral broadening of pulses with output energies beyond 100 mJ at a repetition rate of 5 kHz and showed the compressibility from a pulse duration of 1.3 ps down to 37 fs. This marks, to the best of the authors' knowledge, the highest energy spectrally broadened in a mode preserving system. In comparison to a previous implementation [2], the energy throughput is increased more than 6 times by using a ∼2.7 times longer cell (similar to [3]) and converting the input mode to a first-order Laguerre–Gaussian mode. The output was characterized in detail and shows similar operating figures as the previous configuration [2]. The setup still offers some reserve capacity that might be used to increase the throughput energy even more at the cost of reduced robustness. Alternatively by using helium with above atmospheric pressure in an appropriately designed gas-cell, a further increase of throughput on the order of 40%–70% compared to an argon-based system seems realistic [2]. Under the condition of a well-behaved input mode with excellent symmetry properties, even higher order Laguerre–Gaussian modes can be used [10] with even lower peak intensities creating the possibility of joule class femtosecond laser systems with kilohertz repetition rate.

Funding. Munich-Centre for Advanced Photonics.

Acknowledgment. The authors gratefully acknowledge the support of Prof. Ferenc Krausz, Prof. Matthias Kling, and the *ACCORD* project. Furthermore, we thank Vyacheslav Leshchenko and Alexander Kessel for their help in setting up the vacuum chamber and Yu Chen for manufacturing the optical coatings.

Disclosures. The authors declare no conflicts of interest.

REFERENCES

1. C. Grebing, M. Müller, J. Buldt, H. Stark, and J. Limpert, Opt. Lett. **45**, 6250 (2020).
2. M. Kaumanns, V. Pervak, D. Kormin, V. Leshchenko, A. Kessel, M. Ueffing, Y. Chen, and T. Nubbemeyer, Opt. Lett. **43**, 5877 (2018).
3. M. Kaumanns, V. Pervak, D. Kormin, V. Leshchenko, A. Kessel, Y. Chen, and T. Nubbemeyer, *CLEO Europe and EQEC* (Optical Society of America, 2019), paper Talk cd_9_2.
4. P. L. Kramer, M. K. R. Windeler, K. Mecseki, E. G. Champenois, M. C. Hoffmann, and F. Tavella, Opt. Express **28**, 16951 (2020).
5. P. Balla, A. B. Wahid, I. Sytcevich, C. Guo, A.-L. Viotti, L. Silletti, A. Cartella, S. Alisauskas, H. Tavakol, U. Grosse-Wortmann, A. Schönberg, M. Seidel, A. Trabattoni, B. Manschwetus, T. Lang, F. Calegari, A. Couairon, A. L'Huillier, C. L. Arnold, I. Hartl, and C. M. Heyl, Opt. Lett. **45**, 2572 (2020).
6. M.-W. Lin, T.-Y. Chu, Y.-Z. Chen, D. K. Tran, H.-H. Chu, S.-H. Chen, and J. Wang, Phys. Plasmas **27**, 113102 (2020).
7. R. Behling and F. Grüner, Nucl. Instrum. Methods Phys. Res. A **878**, 50 (2018).
8. N. Milosevic, G. Tempea, and T. Brabec, Opt. Lett. **25**, 672 (2000).
9. R. Paschotta, Opt. Express **14**, 6069 (2006).
10. H. Cao, R. S. Nagymihaly, and M. Kalashnikov, Opt. Lett. **45**, 3240 (2020).
11. R. M. Kaumanns, "Generation of energetic femtosecond pulses at high average power," Ph.D. thesis (Ludwig-Maximilians-Universität, 2020).
12. L. T. Vuong, T. D. Grow, A. Ishaaya, A. L. Gaeta, G. W. 't Hooft, E. R. Eliel, and G. Fibich, Phys. Rev. Lett. **96**, 133901 (2006).
13. S. Ramachandran, J. W. Nicholson, S. Ghalmi, M. F. Yan, P. Wisk, E. Monberg, and F. V. Dimarcello, Opt. Lett. **31**, 1797 (2006).
14. T. Nubbemeyer, M. Kaumanns, M. Ueffing, M. Gorjan, A. Alismail, H. Fattahi, J. Brons, O. Pronin, H. G. Barros, Z. Major, T. Metzger, D. Sutter, and F. Krausz, Opt. Lett. **42**, 1381 (2017).
15. T. M. Kardaś, *Hussar Software* (University of Warsaw, 2018).
16. M. Hanna, X. Délen, L. Lavenu, F. Guichard, Y. Zaouter, F. Druon, and P. Georges, J. Opt. Soc. Am. B **34**, 1340 (2017).
17. S. Zahedpour, J. K. Wahlstrand, and H. M. Milchberg, Opt. Lett. **40**, 5794 (2015).